EARTHQUAKE ENGINEERING AND STRUCTURAL DYNAMICS
Earthquake Engng. Struct. Dyn. **27**, 465–486 (1998)

NUMERICAL SIMULATION OF SUBMARINE PIPELINES IN DYNAMIC CONTACT WITH A MOVING SEABED

C. KALLIONTZIS*†
Computational Hydraulics Office, 70 Omirou Street, Nea Smyrni 17 121, Athens, Greece

SUMMARY

The dynamic response of submarine pipelines to earthquake-generated vertical seabed motions is examined with the aid of a finite element model. A relaxation algorithm is adopted in order to overcome the problem of unknown dynamic seabed reaction forces. Rotational rigidity is assumed at the boundary points, which are allowed to move vertically in unison with the random seabed oscillations. For the interior nodes, the description of the kinetic energy loss, resulting from pipeline–seabed impact, is approached through the use of a restitution coefficient of 0·5, which represents an intermediate collision mode between a perfectly elastic and an inelastic one. Fundamental system frequencies are determined by the use of support positions obtained from a static analysis of the unilaterally constrained structure. The structural damping matrix is approximately evaluated according to Rayleigh's method. Response spectra to a strong motion vertical acceleration earthquake record provide an initial guideline into the pipeline stability. Peak dynamic and static bending stresses are calculated for a case study involving two submarine pipeline crossings. Complete, partial and lack of pipeline gravel cover is assumed in the analysis. A seabed profile alteration, due to probable soil liquefaction, is furthermore imposed, in order to investigate the subsequent effect upon the dynamic pipeline stresses. © 1998 John Wiley & Sons, Ltd.

KEY WORDS: dynamic structural analysis; earthquake motion; finite elements; relaxation solution methods; submarine pipelines; unilateral contact problems

INTRODUCTION

Submarine line structures, such as pipelines or cables, are nowadays routinely laid upon irregular seabed profiles. Identification of the random contact point distribution is of utmost importance in evaluating the peak bending stresses (pipelines) and the maximum suspensions (pipelines and cables). Since deformation takes place pre-dominantly along the vertical plane, one-dimensional analysis proves sufficient for the stability examination of the submarine structures.

So far, the static analysis of unilaterally constrained systems has been the focal point of the majority of research. By transforming the random structure–soil contact problem into a linear complementary one, being equivalent to a strictly convex quadratic programming problem, Maier and Andreuzzi[1] obtained solutions for the relative pipeline–seabed distances. Both elastic and piecewise linear elastoplastic deformation laws were adopted in their model, which was used for obtaining the pipeline bending stresses along the Messina strait crossing. In a similar context, concerning submarine pipelines, the optimal control theory has also been employed by Stavroulakis *et al.*[2] and Chuang and Smith.[3] Bianchi and Oliveri[4] proposed a successive negative reaction node elimination method, capable of yielding the free span pipe lengths along any selected subsea route. Extensive experience of analysing several hundred kilometers of submarine pipe laying was reported. The precision of the bending stress predictions was mainly influenced by the level of

* Correspondence to: C. Kalliontzis, Computational Hydraulics Office, 70 Omirou Street, Nea Smyrni 17 121, Athens, Greece
† Civil Engineer, PhD

CCC 0098–8847/98/050465–22$17·50

Received 14 November 1996
Revised 30 September 1997

accuracy of the seabed profile data. Kalliontzis *et al.* adopted successive over-relaxation using quintic finite elements[5] and non-linear finite differences[6] in order to identify the range of pipeline stresses along the Revithoussa–Aghia Triada strait crossing.

In general, the performance of static analysis alone yields sufficiently accurate results, provided that the structural assembly is situated away from earthquake prone areas. In the latter case, it is imperative to check the response of the structure to dynamic loading, which arises from random earthquake-generated seabed motions. Although there exists an extensive literature on earthquake engineering with respect to buried pipelines, the relevant literature concerning submarine lifelines is rather scarce. Datta and Mashaly[7] used a lumped mass model to evaluate the random response of suspended submarine pipelines to horizontal seismic motions. With the aid of spectral functions, the r.m.s. displacements and stresses were identified in the frequency domain. Romagnoli and Varvelli[8] developed a stochastic Monte-Carlo-type approach coupled with finite element spatial modelling for analysing offshore pipeline and sea floor interactions. Constitutive laws were applied for simulating the seabed motion, whereas the pipeline system response was determined by combining quasi-static and dynamic responses resulting from a stochastic treatment of the equation of motion. The development of approximate analytic small-curvature displacement formulae, enabled Figarov and Kamyshev[9] to obtain stress solutions for buried offshore pipelines, being subjected to seismic excitations.

The problem of submarine lifeline impact upon a moving or stationary seabed, which constitutes the main subject of the present paper, has not been sufficiently addressed. The only relevant dynamic analysis application, that the author is aware of, deals with theoretical cable motions due to a sudden load impact. Avdelas *et. al.*[10] described a mathematical programming technique for investigating the contact–rebound characteristics of a submarine cable-seabed configuration. The imposition of a time variable load function was the cause of cable motion towards a stationary sea floor.

Point iterative numerical solution methods offer generally an efficient calculation approach for the estimation of pipeline profiles in dynamic and/or static random contact with the supporting sea floor. A fully detailed relaxation method is presented herein, being capable of producing bending stress results for a variety of loading and support conditions. Dynamic contact is described with the aid of an average restitution coefficient, thus representing a mean collision mode relative to the two extremes, which involve perfectly elastic and inelastic structural impacts.

In the present study, an amplified strong motion vertical acceleration record[11] is adopted. Seabed soil displacement and velocities are evaluated by solving an equivalent boundary value problem of a Poisson-type equation using Hermite finite elements. Fundamental pipeline system frequencies are approximately determined following a solution of the standard eigenvalue problem, subject to the assumption of known support positions. Knowledge of the static pipeline configurations, yields the necessary positive seabed reaction locations under various loading conditions. This method for estimating the natural frequencies directly implies that the pipeline–seabed contact points remain unaltered during earthquake-generated motions and constitutes an essential assumption that makes tractable an otherwise formidable numerical problem. Based on estimates of the first- and third-mode frequencies the damping matrix is formed using Rayleigh's theory.[12]

The imminent introduction of natural gas in Greece will greatly enhance the economic development of the country. The majority of natural gas (NG) supplies will originate from Russia, whereas secondary reserves will be shipped from Algiers via tankers in liquid form. Specially designed underground tanks for receiving the Algerian Liquid Natural Gas (LNG) are under preparation at the deserted island of Revithoussa. A dual set of concrete-coated submarine steel pipelines will provide the means for transporting the aerated LNG from the Revithoussa island to the mainland at the Aghia Triada peninsula (Figure 1). Currently both pipelines have been successfully installed and tested.

The possibility of partial seabed soil liquefaction following a seismic event led to a three-part design procedure, distinguished mainly by the alternative seabed curves adopted. For the first design stage[6] the natural seabed was used, whereas for the second stage[5] a theoretically optimal seabed profile was generated by removing part of the soft top soil layer, which was considered as being susceptible to liquefaction. In the

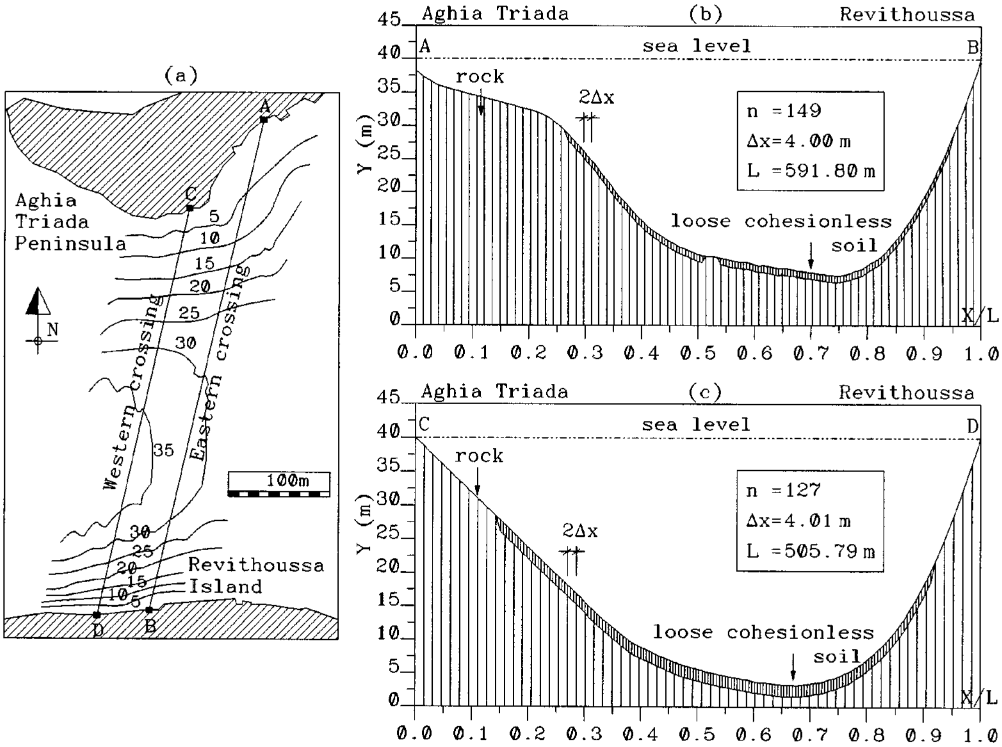

Figure 1. Revithoussa project area plan (a); Eastern (b) and Western (c) crossing natural seabed profiles

third and final design stage the natural seabed was altered according to the second-stage profile specifications, followed by *in situ* irregularity smoothing at critical points.

This paper is mainly focused on the dynamic stress analysis design of the dual submarine lifelines freely resting upon the natural seabed profile. The numerical calculations performed, complement and advance the first design stage[6] investigation for the range of possible peak bending stresses. In addition to simulating the dynamic contact phenomenon with and without pipeline surcharge, the effect of gradual gravel blanket deterioration during an earthquake is also examined. Furthermore, the alteration of the pipe-supporting seabed profile, due to probable soil liquefaction, yields an estimate of the extreme stress development at critical points along the subsea route.

For the analysis of submarine pipelines, stress-based design is usually adopted, instead of the more traditional strain-based design of on-land pipelines. In the latter case, the pipeline is assumed to follow exactly the land topography, i.e. no relative gaps are allowed (full contact hypothesis), unless the pipe is propped using concrete block spacers at regular intervals. As a consequence, standard curve-fitting methods enable the pipe curvatures to be monitored, with a subsequent calculation of bending moments.

Proper surcharge design is of paramount importance for submarine pipeline crossings, particularly when excessive bending stresses due to pressurization are to be curtailed. When used in this context, it is imperative to inspect the submarine pipelines immediately after a seismic event, in order to ascertain that no part of the gravel blanket has disintegrated. In the latter case, corrective measures must be taken by gravel dumping from barges at locations where cover damage is observed. The use of concrete block mattresses, as opposed to rock protection, is a dynamically more stable surcharge alternative option, since greater flexibility is offered during earthquake-generated motions. As a consequence, continuous pipeline coverage is assured at all points.

THEORETICAL ASPECTS

The primary design variable in submarine pipeline analysis is the bending stress. It is, therefore considered as being appropriate to derive the relevant material constitutive law. To achieve this objective, the Kelvin spring-dashpot conceptual model is assumed to capably describe the flexural characteristics at any given pipeline point. The spring stores and releases bending energy during vibration, whereas the dashpot, which represents viscous damping, causes energy dissipation, leading to a structural motion decay. The fundamental stress–strain relationship may then be expressed as

$$\sigma_b = E\left[\varepsilon_b + \beta_d \frac{\partial \varepsilon_b}{\partial t}\right] \tag{1}$$

where E is the Young's modulus, β_d is a viscoelastic (solid) damping coefficient and σ_b and ε_b are the bending stress and bending strain, respectively, defined at the outer pipeline (steel) fibre as

$$\sigma_b = \frac{MR_o}{I}; \quad \varepsilon_b = R_o \frac{\partial^2 y}{\partial x^2} \tag{2}$$

where M is the bending moment, R_o the outer steel pipe radius (Figure 3), y the pipe elevation (Figure 2) and I the composite section moment of inertia, given by

$$\beta = 1 + 2\left[\sin(\alpha)\frac{R_n}{R_i}\right]^2 + \frac{R_n^3 t_e}{\pi R_i^3 t_s}\left[\left(\frac{\pi}{2} - \alpha\right)(1 + 2\sin^2(\alpha)) - \frac{3}{2}\sin(2\alpha)\right] \tag{3}$$

$$\alpha = \frac{2R_n t_e}{\pi(2R_i t_s + R_n t_e)} \tag{4}$$

$$R_n = \tfrac{1}{2}(R_c + R_o) \tag{5}$$

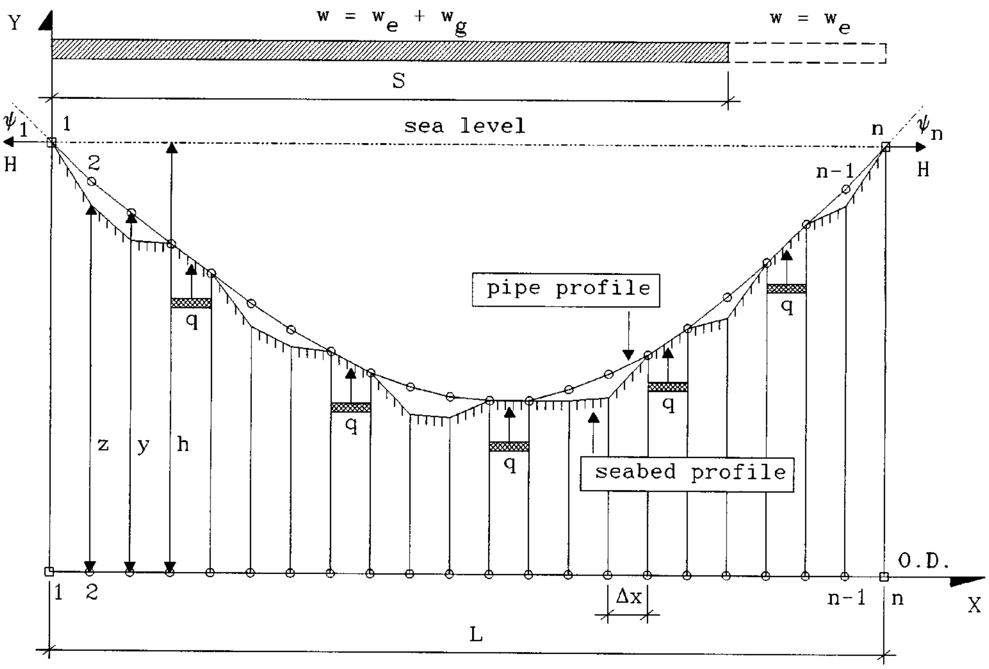

Figure 2. Submarine pipeline–seabed random contact problem definition sketch

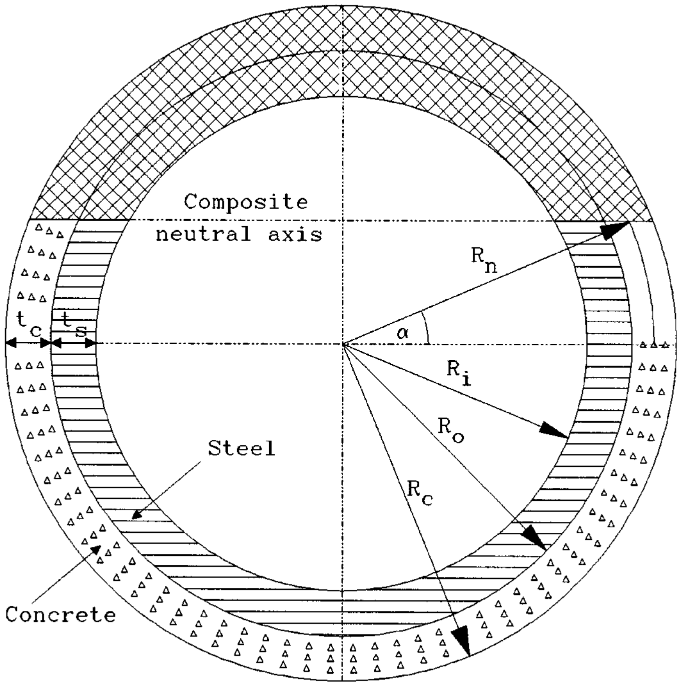

Figure 3. Composite pipeline cross-section

$$t_e = \frac{t_c}{f_e} \tag{6}$$

$$I = \beta \frac{\pi}{4}(R_o^4 - R_i^4) \tag{7}$$

where t_e is the effective concrete thickness, f_e the Young's modulus ratio of steel to concrete (approximately 15), R_i the inner steel radius and R_c the overall pipe radius. Substitution of the stress–strain expressions [equation (2)] into equation (1) leads to

$$M = EI \frac{\partial}{\partial x}\left[\theta + \beta_d \frac{\partial \theta}{\partial t}\right], \quad \theta = \frac{\partial y}{\partial x}, \quad \frac{\partial \theta}{\partial t} = \frac{\partial u}{\partial x} \tag{8}$$

where EI is the composite section stiffness, θ the pipeline gradient (rotation) and u the velocity of structural motion, defined as

$$u = \frac{\partial y}{\partial t} \tag{9}$$

The equation that governs the deformation shape of a submarine pipeline (Figure 2), vibrating in a stationary fluid environment and in random contact with a seabed profile, is given by[13]

$$m\frac{\partial u}{\partial t} + \alpha_d m u + \frac{\partial F}{\partial x} + w_e + w_g - q = 0 \tag{10}$$

where m is the effective structural mass, a sum of the structural and added hydrodynamic masses, α_d the linearized (fluid) damping coefficient, incorporating the hydrodynamically induced structural motion

attenuation mechanism, F the shear force, w_e the effective submarine pipeline weight, w_g the surcharge weight and q the seabed reaction. For linearly elastic slender beams the shear force, including rotation rate damping, may be expressed as

$$F = \frac{\partial M}{\partial x} - H\left[\theta + \beta_d \frac{\partial \theta}{\partial t}\right] \tag{11}$$

where H is the boundary tension. Consequently, equation (10) can be rewritten as

$$m\frac{\partial u}{\partial t} + \left[\alpha_d m u + \beta_d\left(EI\frac{\partial^4 u}{\partial x^4} - H\frac{\partial^2 u}{\partial x^2}\right)\right] + EI\frac{\partial^4 y}{\partial x^4} - H\frac{\partial^2 y}{\partial x^2} + w_e + w_g - q = 0 \tag{12}$$

In the above equation, the expression within the square brackets characterizes 'Rayleigh damping', whereby the first term represents external linear viscous damping due to structural motion within a liquid environment and the second term accounts, firstly, for the internal grain structure damping, specifically, molecular steel friction, and secondly, for the opening/closing process of cracks within the fractured concrete section. The weight w_e and mass m may be determined according to

$$w_e = \pi g[\rho_i R_i^2 + \rho_s(R_o^2 - R_i^2) + \rho_c(R_c^2 - R_o^2) - \rho_o R_c^2] \tag{13}$$

$$m = \frac{w_e}{g} + c_m \rho_o(\pi R_c^2) \tag{14}$$

respectively, where ρ denotes the density, subscripts i,s,c and o referring to the internal pipe fluid, the steel section, the concrete section and the external sea water consecutively, and c_m is the hydrodynamic mass coefficient, taken as 2. For free vibration analysis, the load and damping terms in equation (12) are eliminated and the pipeline elevation is assumed to vary according to

$$y = y_o \sin(\omega t) \tag{15}$$

where y_o is the motion amplitude and ω the oscillation frequency. Substitution of the above equation into equations (9) and (12), respectively, yields after suitable manipulation the following equation, which governs structural free vibrations:

$$-m\omega^2 y_o + EI\frac{\partial^4 y_o}{\partial x^4} - H\frac{\partial^2 y_o}{\partial x^2} = 0 \tag{16}$$

Since the seabed reaction q, which depends both upon x and t, is unknown beforehand, an additional equation is required to enable its determination. Explicit forms are generally unavailable and as a consequence the following condition is usually[1] enforced:

$$(y - z)q = 0 \tag{17}$$

where z is the seabed elevation in reference to an arbitrarily selected ordnance datum and is defined as

$$z(x, t) = z_o(x) + d_z(t) \tag{18}$$

where z_o is the static space-dependent elevation and d_z the vertical time-dependent soil displacement due to an earthquake. The introduction of condition (17), invariably transforms a direct problem into an optimal one. Furthermore, it can readily be seen that equation (17) encompasses both the contact and the suspension possibility of the submarine pipeline relative to the seabed profile. If the seabed reaction is initially assumed to be zero, and a point iterative method[5] is adopted, whereby during calculations the pipe elevation y is restrained from being assigned a value less than or equal to the seabed elevation z, then the implementation of condition (17) becomes redundant. To apply such a technique in a dynamic analysis context, absolute and

not relative pipeline motions with respect to the vibrating seabed must be considered. Relative structural motions due to earthquakes[12] are generally applicable when support locations are well defined. Submarine pipeline–seabed interactions during seismic excitation involves complex impact and rebound phenomena at random positions, thus precluding direct methods of dynamic analysis.

In submarine pipeline systems, which are restrained from axial movement, a tensile force H develops at the boundaries. The assumption of linear Euler beam theory implies that this force is equally transmitted at every point within the structure. Depending on the loading conditions, the expression for H assumes the following form:

$$H = H_{\mathrm{p}} + H_{\mathrm{a}} + \Delta H_{\mathrm{a}} + H_{\mathrm{d}} \tag{19}$$

where H_{p} is a tension component due to the Poisson effect, H_{a} an additional tensile or compressive force,[14] due to structural loading or unloading, respectively, ΔH_{a} an incremental axial (usually tensile) force, due to pipeline profile deviations from static equilibrium, and H_{d} the dynamic tension,[15] introduced whilst the pipeline vibrates relative to an original configuration.

The Poisson effect tension may be written as

$$H_{\mathrm{p}} = \frac{1}{L}\int_0^L 2\mu(p_{\mathrm{i}}A_{\mathrm{i}} - p_{\mathrm{o}}A_{\mathrm{o}})\,\mathrm{d}x = 2\mu p_{\mathrm{i}}A_{\mathrm{i}} - 2\mu\rho_{\mathrm{o}}gA_{\mathrm{o}}\left(h - \frac{1}{L}\int_0^L y\,\mathrm{d}x\right) \tag{20}$$

where μ is the Poisson ratio for steel, A_{i} and A_{o} the inner and outer steel pipe areas, p_{i} the internal liquid or gas pressure and p_{o} the external hydrostatic pressure. The equation for the axial forces H_{a}, ΔH_{a} and H_{d} is similar in form, since it represents axial motion restraint of the structural assembly. Hence, a typical formula for the dynamic tension is

$$H_{\mathrm{d}} = EA\frac{(J - J_{\mathrm{s}})}{L} \tag{21}$$

where $A\ (=A_{\mathrm{o}} - A_{\mathrm{i}})$ is the steel cross-sectional area and subscript s denotes a reference level, for instance, the original as laid pipe profile in a static situation or the static equilibrium in a dynamic situation. The length variable J must then be interpreted in an independent way according to the loading condition under investigation, and is generally defined as

$$J = \frac{1}{2}\int_0^L \theta^2\,\mathrm{d}x \tag{22}$$

Impact and rebound between two structural objects moving at different velocities may be described with the aid of the restitution equation, which in the present case has the following form:

$$(u^{t+\Delta t} - v_z^{t+\Delta t}) + c_{\mathrm{R}}(u^t - v_z^t) = 0 \tag{23}$$

where c_{R} is the restitution coefficient, v_z the seabed velocity and Δt a small time increment. For a perfectly elastic collision, a situation unattainable in practice, c_{R} must be assigned a value of unity, whereas a zero value for c_{R} represents inelastic collision, whereby the pipeline sticks to the seabed after impact and moves accordingly in unison.

The von Mises equivalent stress concept[16] is used for establishing the acceptable levels of pipeline flexural stability. As a consequence the following stress constraint is imposed:

$$\max\{\sigma_{\mathrm{e}}^{\mathrm{I}}, \sigma_{\mathrm{e}}^{\mathrm{II}}\} \leqslant \eta\sigma_{\mathrm{y}} \tag{24}$$

where σ_{e} is the equivalent stress, σ_{y} the yield stress of steel and η a usage factor, which assumes a value of less than or equal to unity. The superscripts I and II in equation (24) correspond to the tensile and compressive bending stress development at the end fibres of the beam section. The appropriate equivalent

stress formulae are

$$\begin{aligned}\sigma_{\mathrm{e}}^{\mathrm{I}} &= \sqrt{(\sigma_{\mathrm{t}} + f_{\mathrm{b}}|\sigma_{\mathrm{b}}|)^2 + \sigma_{\mathrm{h}}^2 - (\sigma_{\mathrm{t}} + f_{\mathrm{b}}|\sigma_{\mathrm{b}}|)\sigma_{\mathrm{h}}} \\ \sigma_{\mathrm{e}}^{\mathrm{II}} &= \sqrt{(\sigma_{\mathrm{t}} - f_{\mathrm{b}}|\sigma_{\mathrm{b}}|)^2 + \sigma_{\mathrm{h}}^2 - (\sigma_{\mathrm{t}} - f_{\mathrm{b}}|\sigma_{\mathrm{b}}|)\sigma_{\mathrm{h}}}\end{aligned} \tag{25}$$

where f_{b} is a stress factor ranging from 0·85 to 1·0 and σ_{h} and σ_{t} are the hoop and tensile stresses, respectively, given by

$$\sigma_{\mathrm{h}} = \frac{H_{\mathrm{p}}}{\mu A}, \quad \sigma_{\mathrm{t}} = \frac{H}{A} \tag{26}$$

Based on equations (24) and (25), the validity of the numerically calculated bending stresses can then be directly checked[17] according to

$$\begin{aligned}|\sigma_{\mathrm{b}}| &\leqslant \min\left\{\frac{\sigma_{\mathrm{b}}^{\mathrm{I}}}{f_{\mathrm{b}}}, \frac{\sigma_{\mathrm{b}}^{\mathrm{II}}}{f_{\mathrm{b}}}\right\} \\ \sigma_{\mathrm{b}}^{\mathrm{I}} &= \tfrac{1}{2}[\sigma_{\mathrm{h}} + \sqrt{4(\eta\sigma_{\mathrm{y}})^2 - 3\sigma_{\mathrm{h}}^2}] - \sigma_{\mathrm{t}} \\ \sigma_{\mathrm{b}}^{\mathrm{II}} &= \tfrac{1}{2}[-\sigma_{\mathrm{h}} + \sqrt{4(\eta\sigma_{\mathrm{y}})^2 - 3\sigma_{\mathrm{h}}^2}] + \sigma_{\mathrm{t}}\end{aligned} \tag{27}$$

NUMERICAL PROCEDURES

Finite element discretization

The horizontal distance spanning a typical submarine pipeline crossing (Figure 2) is subdivided into a pre-selected number of equally Δx-spaced finite elements. Within each element, cubic Hermite polynomial functions are adopted for representing the spatial variation of the pipe elevation y. Application of the virtual work principle on an element basis[18] enables the transformation of equation (12) into

$$[M]\left\{\frac{\partial V}{\partial t}\right\} + [C]\{V\} + [K]\{Y\} + \{W\} = \{F\} \tag{28}$$

where $[M]$ is the mass matrix, $[C]$ the damping matrix, $[K]$ the augmented stiffness matrix, including tensile force effects, $\{W\}$ the load vector and $\{F\}$ the element force vector. With the aid of the beam element discretization variables, i.e. pipe elevation y and rotation θ, the structural velocity u [equation (9)] can be expressed in vectorial form as

$$\left\{\frac{\partial Y}{\partial t}\right\} = \{V\} \tag{29}$$

The matrices and vectors in equations (28) and (29) are explicitly defined according to

$$[M] = \left[\begin{array}{cc|cc} a_1 & a_2 & a_3 & a_4 \\ & a_5 & -a_4 & a_6 \\ \hline & & a_1 & -a_2 \\ \mathrm{Sym} & & & a_5 \end{array}\right], \quad [K] = \left[\begin{array}{cc|cc} b_1 & b_2 & b_3 & b_4 \\ & b_5 & -b_4 & b_6 \\ \hline & & b_1 & -b_2 \\ \mathrm{Sym} & & & b_5 \end{array}\right] \tag{30}$$

$$\{W\} = \frac{(w_{\mathrm{e}} + w_{\mathrm{g}})\Delta x}{12}\{6 \ \Delta x \vdots 6 \ -\Delta x\}^{\mathrm{T}} \tag{31}$$

$$\{F\} = \{F_1 \quad M_1 \vdots F_2 \quad M_2\}^{\mathrm{T}} \tag{32}$$

$$\{Y\} = \{y_1 \quad \theta_1 \vdots y_2 \quad \theta_2\}^{\mathrm{T}} \tag{33}$$

$$\{V\} = \{u_1 \quad v_1 \vdots u_2 \quad v_2\}^{\mathrm{T}} \tag{34}$$

where subscripts 1 and 2 denote the left and right nodes, respectively, of a finite element and v is the temporal rate of change of the rotation θ. Furthermore, the mass and stiffness matrix coefficients are given by

$$\{a\} = \frac{m\Delta x}{420}\begin{Bmatrix} 156 \\ 22\Delta x \\ 54 \\ -13\Delta x \\ 4\Delta x^2 \\ -3\Delta x^2 \end{Bmatrix}, \quad \{b\} = \frac{2EI}{\Delta x^3}\begin{Bmatrix} 6 \\ 3\Delta x \\ -6 \\ 3\Delta x \\ 2\Delta x^2 \\ \Delta x^2 \end{Bmatrix} + \frac{H}{30\Delta x}\begin{Bmatrix} 36 \\ 3\Delta x \\ -36 \\ 3\Delta x \\ 4\Delta x^2 \\ -\Delta x^2 \end{Bmatrix} \tag{35}$$

It may be observed that the seabed reaction q has been purposely excluded from the load vector $\{W\}$. If reaction values are required, then these may be calculated by simple addition of shear forces,[5] after obtaining a solution for the unknown displacements.

Evaluation of damping

A direct calculation of the damping matrix $[C]$ is not possible, since the damping coefficients α_d and β_d are not known or cannot be evaluated with certainty. However, if the damping matrix is ignored altogether from the structural analysis, a hypothesis which is equivalent to eliminating the friction in hydraulic analysis of pipelines, then a mechanism is lacking for achieving a statically equivalent equilibrium. More specific, dynamic relaxation of structural systems cannot be performed. As a consequence, Rayleigh's theory is adopted herein in order to obtain at least an estimate of the components of the damping matrix coefficients. Application of the finite element principles on the relevant term (within square brackets) in equation (12) leads to

$$[C] = \alpha_d[M] + \beta_d[K] \tag{36}$$

The damping parameters can be evaluated according to[12]

$$\alpha_d = \frac{2\xi\omega_1\omega_3}{\omega_1 + \omega_3}, \quad \beta_d = \frac{2\xi}{\omega_1 + \omega_3} \tag{37}$$

in which ω_1 and ω_3 are the first- and third-mode frequencies, respectively, and ξ is an assumed damping ratio. Increased damping of higher mode frequencies appears by use of formulae (37) and as a result this method of determining the damping matrix must be considered only as approximate. The fundamental system frequencies ω are determined by solving a standard[18] eigenvalue problem, resulting from the discrete representation of equation (16). The basic assumption of known pipeline–seabed contact points is invoked, whereby a static solution of the unilaterally constrained structure provides the required support locations.

Finite difference temporal integration

Equations (28) and (29) represent a set of first-order differential equations in time, for the numerical integration of which the Crank–Nicolson central weighting scheme is employed. Consequently,

$$\frac{1}{\Delta t}[M]\{V^{k+1} - V^k\} + \tfrac{1}{2}[C]\{V^{k+1} + V^k\} + \tfrac{1}{2}[K]\{Y^{k+1} + Y^k\} + \{W\} = \{\bar{F}\} \tag{38}$$

$$\frac{1}{\Delta t}\{Y^{k+1} - Y^k\} = \tfrac{1}{2}\{V^{k+1} + V^k\} \tag{39}$$

where k is a time level index and $\{\bar{F}\}$ a mean element force vector. It may be observed that equation (39) corresponds exactly to the Newmark scheme[12] by adopting the parameters $(\frac{1}{2}, \frac{1}{4})$ and eliminating the acceleration terms. Further rearrangement of equation (39) yields

$$\{V^{k+1}\} = \frac{2}{\Delta t}\{Y^{k+1} - Y^k\} - \{V^k\} \tag{40}$$

Subsequent substitution of equation (40) into equation (38) leads to

$$[D]\{Y^{k+1}\} + \{P\} = \{\bar{F}\} \tag{41}$$

$$[D] = \frac{1}{2}[K] + \frac{1}{\Delta t}[C] + \frac{2}{\Delta t^2}[M] \tag{42}$$

$$\{P\} = \left(\frac{1}{2}[K] - \frac{1}{\Delta t}[C] - \frac{2}{\Delta t^2}[M]\right)\{Y^k\} - \frac{2}{\Delta t}[M]\{V^k\} + \{W\} \tag{43}$$

The above equations constitute a numerical integration scheme, which offers unconditional stability. This implies, that in theory at least, large time steps can be adopted without major deviations from the expected overall response characteristics of the structure to a given dynamic excitation. However, significant loss of accuracy may be expected, and is therefore advisable to keep time steps as low as possible, in order to properly model all intricate structural deformations, particularly when seismic motions are involved in conjunction with impact and rebound phenomena.

Point relaxation strategy

Instead of proceeding in the familiar way of element assembly and solution[18] (coupled with an optimization procedure), a nodal formulation technique is adopted herein, being closely linked with the proposed point iterative solution algorithm. In this respect, the use of an equal element length subdivision enables a direct development of nodal formulae at the three characteristic nodes of the discretized structural system, which comprises the two boundary nodes (left–right points) and the group of interior nodes. Prior to the detailed presentation of the nodal equations, a set of additional matrix coefficients must be defined. In vectorial form, these are

$$\{d\} = \frac{1}{2}\{b\} + \frac{1}{\Delta t}(\alpha_{\rm d}\{a\} + \beta_{\rm d}\{b\}) + \frac{2}{\Delta t^2}\{a\} \tag{44}$$

Consequently, the appropriate nodal formulae, which correspond to the three characteristic nodes, may be written in residual form as follows

Interior node

$$\begin{aligned} r_{i,1} &= d_3(y_{i+1}^{k+1} + y_{i-1}^{k+1}) + 2d_1 y_i^{k+1} + d_4(\theta_{i+1}^{k+1} - \theta_{i-1}^{k+1}) + p_{i,1} \\ \Delta y_i &= \frac{r_{i,1}}{2d_1} \end{aligned} \qquad (y - \text{equ.}) \tag{45}$$

$$\begin{aligned} r_{i,2} &= d_4(y_{i-1}^{k+1} - y_{i+1}^{k+1}) + 2d_5\theta_i^{k+1} + d_6(\theta_{i+1}^{k+1} + \theta_{i-1}^{k+1}) + p_{i,2} \\ \Delta \theta_i &= \frac{r_{i,2}}{2d_5} \end{aligned} \qquad (\theta - \text{equ.}) \tag{46}$$

Left node ($i = 1$)

$$\left.\begin{aligned} r_{i,1} &= d_1 y_i^{k+1} + d_2 \theta_i^{k+1} + d_3 y_{i+1}^{k+1} + d_4 \theta_{i+1}^{k+1} + p_{i,1} \\ \Delta y_i &= \frac{r_{i,1}}{d_1} \end{aligned}\right\} \quad (y - \text{equ.}) \qquad (47)$$

$$\left.\begin{aligned} r_{i,2} &= d_2 y_i^{k+1} + d_5 \theta_i^{k+1} - d_4 y_{i+1}^{k+1} + d_6 \theta_{i+1}^{k+1} + p_{i,2} \\ \Delta \theta_i &= \frac{r_{i,2}}{d_5} \end{aligned}\right\} \quad (\theta - \text{equ.}) \qquad (48)$$

Right node ($i = n$)

$$\left.\begin{aligned} r_{i,1} &= d_3 y_{i-1}^{k+1} - d_4 \theta_{i-1}^{k+1} + d_1 y_i^{k+1} - d_2 \theta_i^{k+1} + p_{i,1} \\ \Delta y_i &= \frac{r_{i,1}}{d_1} \end{aligned}\right\} \quad (y - \text{equ.}) \qquad (49)$$

$$\left.\begin{aligned} r_{i,2} &= d_4 y_{i-1}^{k+1} + d_6 \theta_{i-1}^{k+1} - d_2 y_i^{k+1} + d_5 \theta_i^{k+1} + p_{i,2} \\ \Delta \theta_i &= \frac{r_{i,2}}{d_5} \end{aligned}\right\} \quad (\theta - \text{equ.}) \qquad (50)$$

where vector components $p_{i,1}$ and $p_{i,2}$ are evaluated with the aid of equations (43). Estimates of variables y^{k+1} and θ^{k+1} may be obtained, either following a static solution of the unilateral contact problem (for the second time level), or from the previous time step solutions. New values are then computed according to

$$\begin{Bmatrix} y_i^{k+1} \\ \theta_i^{k+1} \end{Bmatrix}^{\text{new}} = \begin{Bmatrix} y_i^{k+1} \\ \theta_i^{k+1} \end{Bmatrix}^{\text{old}} - r_{\text{f}} \begin{Bmatrix} \Delta y_i \\ \Delta \theta_i \end{Bmatrix} \qquad (51)$$

subject to the elevation constraint of

$$\text{If } (y_i^{k+1})^{\text{new}} \leqslant z_i \text{ then set } (y_i^{k+1})^{\text{new}} = z_i \qquad (52)$$

In equation (51), r_{f} is a relaxation factor, which can be determined through numerical experimentation. For static analysis a value of 1·97 is appropriate,[5] whereas for dynamic analysis a value of 1·0 yields generally optimal performance, and is therefore recommended. The iterative procedure governed by equations (45)–(52), is repeatedly applied until the following convergence criterion is reached:

$$\sqrt{\{r\}^{\text{T}}\{r\}} \leqslant \varepsilon \qquad (53)$$

where ε is a tolerance criterion specified beforehand. Although a value of 0·001 offers suitable convergence characteristics in a static analysis context, when dynamic calculations are carried out, then the tolerance limit must be significantly reduced, in order to obtain accurate results. A suggested ε value is 0·000001. Appropriate boundary formula selection depends on the end conditions of the structural system. A variety of situations may be modelled, for instance, simple or fixed end supports, which involve the θ-variables, and rollers, which involve the y-variables and are only applicable when a dynamic analysis is performed. Use of the roller end condition is not advisable, since the local impact–rebound phenomena at the end points, generate spurious longitudinal elastic waves, corrupting in the process the numerical solution. Once a solution for $\{Y^{k+1}\}$ is available, equations (41) are utilized for providing the necessary shear force and bending moment values.

Pipeline impact upon the seabed

The relative position of the pipeline with respect to the seabed profile, dictates the method of calculation of the velocities u^{k+1} at the next time level. Two cases are possible, one whereby the structural system is suspended and another whereby the pipeline is in contact with the seabed. In the first case equations (40) provide the necessary velocities, whereas in the second case equation (23) yields the appropriate rate of change of y, the magnitude of which is dictated by the form of collision. Impact phenomena may be described through use of either an elastic or a plastic theory. For an elastic impact the sign of the relative pipeline–seabed velocity is reversed. This represents an ideal situation unattainable in practice, since no kinetic energy loss or instantaneous localized shape distortion due to collision is allowed. According to plastic impact theory, the relative velocity becomes zero after collision, causing a temporary adherence between the pipeline and the seabed. Separation can then only take place, when pipe raising conditions prevail at points in close proximity to the contact area.

The random texture of the seabed soil surface, which ranges from hard rock, with c_R probably higher than 0·5, to loose cohesionless soil, with c_R lower than 0·5 (in parts close to zero), precludes an accurate prediction of the restitution coefficient. As a consequence, an average collision mode ($c_R = 0{\cdot}5$) is assumed in the present theory. For a stationary seabed, this c_R value represents a 75 per cent loss in kinetic energy following impact. Numerical results tend to be relatively unaffected by the judicial choice of the restitution coefficient values.

Tensile force calculation

The presence of boundary tensions due to internal pressure (Poisson effect) and axial pipeline restraint, introduces a non-linearity into the numerical analysis, which is more pronounced in static profile calculations. The contribution of the Poisson effect tension, as far as the non-linearity is concerned, is relatively low. Consequently, an approximate calculation of the integral expression of equation (20) is facilitated, whereby the seabed profile data are used in place of the pipeline elevation. However, the most significant tensile force non-linearity arises, when a load is either imposed upon the structure (i.e. internal fluid introduction leading to H_a tensile) or released therefrom (i.e. internal fluid removal leading to H_a compressive). Alternatively, similar non-linearities appear in relation to incremental tensile forces ΔH_a, which develop when sections of the supporting seabed are displaced due to subsoil subsidence. In this case an iterative under-relaxation scheme proves efficient for the evaluation of the axial boundary forces (H_a or ΔH_a). Hence,

$$H_a^{j+1} = H_a^{j-1} + \zeta(H_a^j - H_a^{j-1}) \tag{54}$$

where j is the iteration level and ζ is an under-relaxation factor, which is problem dependent and ranges from as low as 0·01 up to 0·25 (and under certain circumstances 0·50). To obtain an optimal parameter, a search initiation from 0·01 and upwards is suggested, always checking the convergence characteristics and the associated solution speed. Convergence is assumed to be reached, when the percentage change in successive iterations falls below a value of 0·005. With the aid of the cubic finite element polynomials, the integral of equation (22) can be explicitly determined according to

$$\begin{aligned} J &= \frac{1}{2}\sum_{e} J_e \\ J_e &= \frac{6}{5\Delta x}(y_1 - y_2)^2 + \frac{1}{5}(y_1 - y_2)(\theta_1 + \theta_2) + \frac{2\Delta x}{15}(\theta_1 + \theta_2)^2 - \frac{\Delta x}{3}\theta_1\theta_2 \end{aligned} \tag{55}$$

where subscript e denotes an element. Although the dynamic tensions, which develop during pipeline vibrations, are non-linear, these may be approximately estimated, using variable information from the previous time level. This approach yields acceptable tensions H_d, as long as the time step for advancing the calculations is kept low. In the present study, the specification of small Δt values, which are deemed necessary for an adequate description of the seismic acceleration record, cover the aforementioned prerequisite.

Seabed seismic motion

Earthquake-generated motions are generally available as acceleration records. Since accurate ground displacements and velocities are required for the determination of, firstly, the absolute seabed elevation motion [equation (18)], and secondly, the structural pipe velocity after impact [equation (23)], a boundary value problem is solved using the following Poisson-type equation

$$-\frac{\mathrm{d}^2}{\mathrm{d}t^2}(d_z) + a_z = 0 \tag{56}$$

where a_z is the vertical component of the ground acceleration. It can readily be seen that equation (56) is mathematically equivalent to a cable structure being subjected to a unit tension and carrying a linearly variable load. By using cubic Hermite polynomial time functions, the local finite element equations can be explicitly written as

$$\frac{1}{30\Delta t}\left[\begin{array}{cc:cc} 36 & 3\Delta t & -36 & 3\Delta t \\ & 4\Delta t^2 & -3\Delta t & -\Delta t^2 \\ \hdashline & & 36 & -3\Delta t \\ \text{Sym} & & & 4\Delta t^2 \end{array}\right]\left\{\begin{array}{c} d_{z1} \\ v_{z1} \\ \cdots \\ d_{z2} \\ v_{z2} \end{array}\right\} + \frac{a_{z1}\Delta t}{12}\left\{\begin{array}{c} 6 \\ \Delta t \\ \cdots \\ 6 \\ -\Delta t \end{array}\right\} + \frac{(a_{z2}-a_{z1})\Delta t}{60}\left\{\begin{array}{c} 9 \\ 2\Delta t \\ \cdots \\ 21 \\ -3\Delta t \end{array}\right\} = 0 \tag{57}$$

The ground displacements d_z and velocities v_z are subsequently identified by employing standard element assembly procedures,[18] followed by imposition of zero-displacement values at the time boundaries.

REVITHOUSSA CASE STUDY

Generalities

The future introduction of natural gas in Greece constitutes one of the largest investments in energy resources in this country during the recent decades, with an estimated overall cost of 2·5 billion dollars. The State owned (Public Gas Corporation [DEPA]) natural gas system will be capable of storing and transmitting quantities of the order of 3·0 billion m^3 per year, of which 80 per cent will originate from Russia, whereas 20 per cent will be shipped from Algiers to Revithoussa island in liquid form. As a consequence, the construction on the island of Revithoussa of a liquid natural gas (LNG) terminal complex was planned, in order to meet the predicted increased future demand in natural gas supplies for the general Athens area, particularly during the winter season. Amongst other installations, the complex includes two 65 000 m^3 capacity storage tanks for receiving the Algerian LNG and docking facilities for tankers of 25 000–50 000 m^3 capacity. The Algerian LNG will in the process be transformed into natural gas (NG) and directed at high pressures (70 bar) through a pair of submarine pipelines towards the mainland at Aghia Triada. A plan of the project area, including the relevant cross-sections concerning the Eastern and Western pipeline crossings is illustrated in Figure 1. The terminal station, the cost of which is estimated at 0·5 billion dollars, is expected to be fully operational by the end of 1998.

Currently, DEPA is developing plans for the future introduction of Norwegian natural gas, passing through France and Italy, and eventually being transported to Greece via a 120 km long submarine pipeline (estimated cost 0·4 billion dollars), connecting Otranto (Italy) to Igoumenitsa (Greece) (operational target: 2001–2002). Furthermore, the possibility of Norwegian LNG transportation using tankers from North Sea through Gibraltar to Greece is also under investigation. Additionally, the probability of augmenting the natural gas supplies with Iranian gas is also taken into consideration.

Seismic excitation

Earthquake-resistant pipeline design was carried out in accordance with the New Hellenic (Greek) Anti-seismic Code (NEAC; October 1992 plus amendments of June 1995), which has been enforced since July 1995. Based on NEAC, Greece is divided into four zones of increasing seismic hazard. Revithoussa island lies on the border of zones II and III, between Athens and the eastern part of the gulf of Corinth, where large magnitude earthquakes have taken place in the past, the most recent being that of February 1981 (surface seismic wave magnitude $M_s = 6{\cdot}7$; PGA $= 0{\cdot}29g$; $a_z = 0{\cdot}10g$; macroseismic Mercalli scale intensity $I_s = 9$). Due to project importance, the Revithoussa–Aghia Triada crossing area was assumed to belong to zone III with a characteristic horizontal peak ground acceleration (PGA) of $0{\cdot}24g$. For the prediction of the maximum vertical acceleration, the code recommends a 30 per cent reduction of the horizontal PGA. Consequently a value of a_z equal to $0{\cdot}17g$ was adopted in the present study.

Although there are many records available, the author selected the data given in reference 11, mainly due to their long duration period, as compared to existing earthquake acceleration graphs in Greece. The original vertical acceleration data were scaled from a peak value of $0{\cdot}07g$–$0{\cdot}17g$ (Figure 4). Ground displacements and velocities were subsequently computed with the aid of the assembled form of equations (57). The pseudo-acceleration S_a response spectrum was next constructed, by determining, for a given natural vibration period T_n and damping ratio ξ, the peak relative displacement r_o using a direct integration method proposed by Chopra[12] for the solution of the linear viscoelastic SDF system

$$\frac{d^2r}{dt^2} + 2\xi\omega_n\frac{dr}{dt} + \omega_n^2 r = -a_z; \quad \omega_n = \frac{2\pi}{T_n}; \quad S_a = \omega_n^2 r_o \tag{58}$$

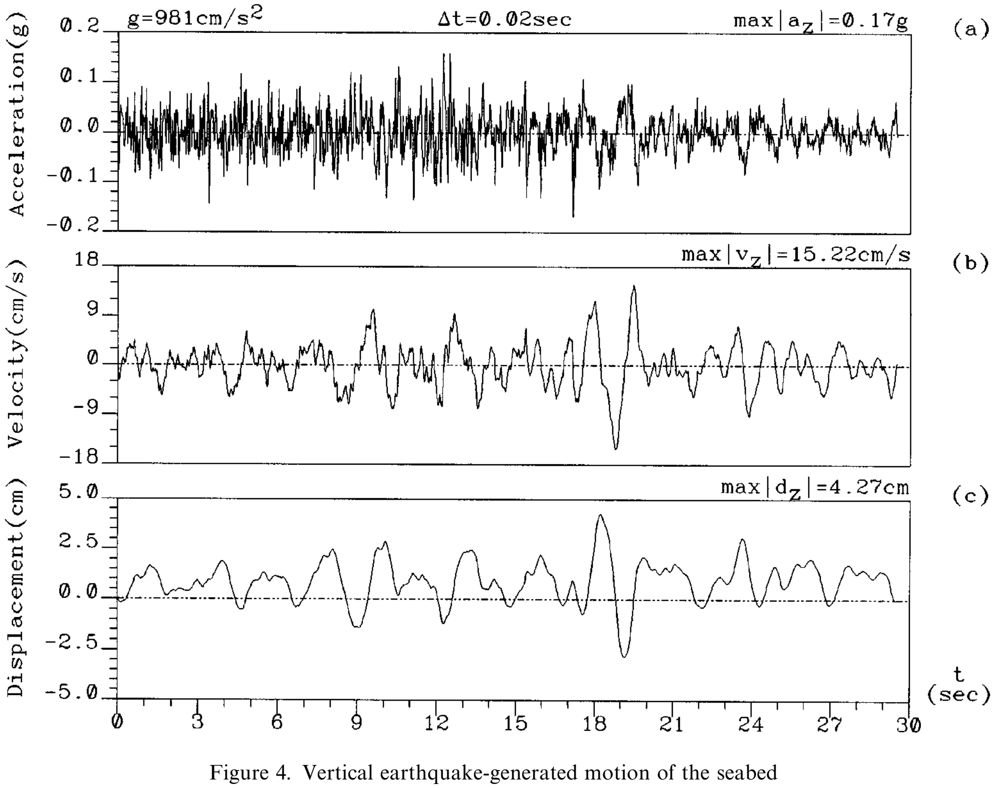

Figure 4. Vertical earthquake-generated motion of the seabed

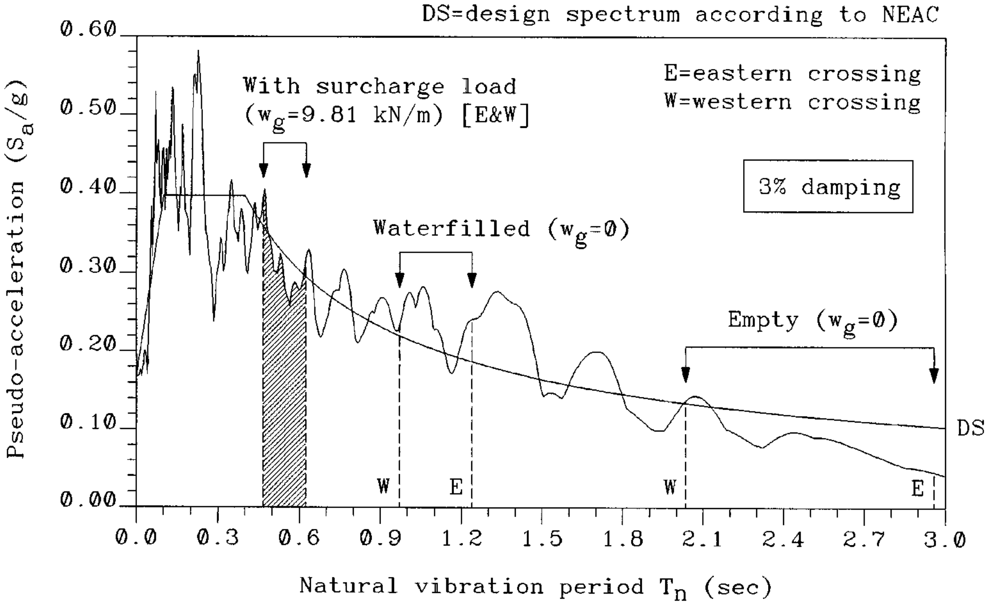

Figure 5. Pseudo-acceleration response spectrum and pipeline vibration periods corresponding to the natural seabed profile

where r is the mass-support relative displacement and ω_n the natural system frequency. An illustration of this graph, together with the relevant design spectrum based on the proposals of NEAC, is presented in Figure 5. The code suggests damping ratios of 5 per cent for reinforced concrete and 2 per cent for welded steel. Since the submarine pipeline is composite (Figure 3), a damping ratio of 3 per cent was utilized in all subsequent calculations.

Approximate pipeline vibration periods were estimated by first assuming that the contact points, as obtained from a static analysis, were known beforehand. This enabled the solution of the standard eigenvalue problem [equation (16)] for all possible loading cases. Fundamental pipeline parametric data are given in Table I, whereas in Table II all relevant parameters for the six loading cases pertinent to the installation phase of the pipelines are presented. Table II includes also the system frequencies corresponding to the natural seabed profiles.

Table I. Pipeline data

Parameter	Value
Composite stiffness, EI	264 513 kNm^2
Moment of inertia, I	128 398 cm^4
Axial rigidity, EA	4 909 468 kN
Section modulus, I/R_o	4 210 cm^3
Yield stress of steel, σ_y	448 N/mm^2
Poisson ratio of steel, μ	0·30
Outer steel pipe radius, R_o	30·50 cm
Steel wall thickness, t_s	1·27 cm
Concrete thickness, t_c	6·00 cm
Test pressure p_i	105 bar
Gravel surcharge, w_g	9·81 kN/m

Table II. Installation scheme parameters [the frequencies ω (rad/s) correspond to the natural seabed profile]

No.	Loading case	S/L	w_e (kN/m)	m (t/m)	η	East ω_1/ω_3	West ω_1/ω_3
1	Empty	0·0	0·476	0·907	0·72	2·125/3·540	3·087/6·437
2	Water filled	0·0	3·109	1·175	0·72	5·075/6·301	6·470/8·314
3	Pressure test	0·0	3·109	1·175	0·96	0·654/1·695	0·616/2·065
4	Empty	1·0	0·476	0·907	0·72	13·317/20·759	11·403/21·731
5	Water filled	1·0	3·109	1·175	0·72	13·476/15·716	10·052/21·743
6	Pressure test	1·0	3·109	1·175	0·96	12·548/14·905	11·026/18·025

Table III. Eastern crossing result summary [natural seabed profile; $|\sigma_b|$ in (N/mm^2) and H_d in (kN); $\Delta H_a = 0$ (kN)]

	Static analysis				Dynamic analysis	
No.	H_p (kN)	H_a (kN)	J_s (m)	$\max\lvert\sigma_b\rvert/\lim\lvert\sigma_b\rvert$	$\min H_d/\max H_d$	$\max\lvert\sigma_b\rvert/\lim\lvert\sigma_b\rvert$
1	−35	−128	6·358157	211·48/318·14	−106/56	243·29/318·41
2	0	0	6·373599	234·82/322·56	−71/62	253·80/321·65
3	1656	0	5·459781	497·09/334·11	−279/289	530·87/340·90
4	−35	−12	6·391976	280·53/322·06	−12/9	292·09/321·94
5	0	0	6·393447	286·85/322·56	−10/12	306·66/322·37
6	1656	0	6·389950	297·29/334·11	−18/20	311·70/334·52

Once an estimate of the structural period is made available, the load factor λ ($=S_a/g$) can be determined from Figure 5 and subsequently used in a quasi-static equivalent transformation of the actual dynamic problem. Thus, a preliminary insight into the dynamic stability of the structure is made possible. High sagbend and overbend stress problems can be identified (+ve λ), in addition to instantaneous floatation possibilities (−ve λ), being followed by pipeline impact upon the seabed. Although the finite element model is capable of performing quasi-static analyses, such results are not presented herein, since the primary concern of this study, is the dynamic response of line structures to probable strong motion earthquakes.

Installation stresses

A peak dynamic and static bending stress investigation was carried out for the dual submarine pipeline crossing. The natural seabed profile was adopted in all calculations. Two major design aspects are distinguished, one whereby no surcharge is imposed (loading cases 1, 2 and 3) and another whereby the pipelines are fully covered by gravel (loading cases 4, 5 and 6). For both design approaches, the pipeline end points were assumed to be fixed after waterfilling, thus yielding the end rotation values ($\theta_1 = \tan(\psi_1)$; $\theta_n = \tan(\psi_n)$) and J_s the reference length variable for the calculation of the axial compressive force after liquid removal from the pipelines. Typical stress results for the Eastern and Western crossings are given in Tables III and V, respectively. A value of 1·0 was assigned to the bending stress factor f_b.

The free laying of the pipelines upon the natural seabed, led to impermissible bending stresses for the pressure test case (Figure 6) at the Revithoussa island boundary. Since an intervention upon the steep

Table IV. Eastern crossing result summary [liquefaction altered seabed profile; $|\sigma_b|$ in (N/mm^2) and H_d in (kN); H_p and H_a same as in Table III; ω in (rad/s)]

	Static analysis			Dynamic analysis		
No.	ΔH_a (kN)	J_s (m)	$\max\|\sigma_b\|/\lim\|\sigma_b\|$	ω_1/ω_3	$\min H_d/\max H_d$	$\max\|\sigma_b\|/\lim\|\sigma_b\|$
1	301	6·394555	213·53/314·28	0·345/0·863	−322/351	239·39/308·47
2	1146	6·512003	417·26/274·47	0·679/1·478	−329/443	441·50/265·12
3	223	5·486702	598·57/343·46	0·704/1·473	−210/289	632·08/342·19
4	3297	6·789758	606·70/183·71	2·088/6·224	−184/179	627·10/180·80
5	3705	6·840487	659·48/167·08	2·377/5·706	−170/183	687·25/162·64
6	2768	6·723859	675·28/310·62	1·555/5·168	−260/258	696·52/305·34

Table V. Western crossing result summary [natural seabed profile; $|\sigma_b|$ in (N/mm^2) and H_d in (kN); $\Delta H_a = 0$ (kN)]

	Static analysis				Dynamic analysis	
No.	H_p (kN)	H_a (kN)	J_s (m)	$\max\|\sigma_b\|/\lim\|\sigma_b\|$	$\min H_d/\max H_d$	$\max\|\sigma_b\|/\lim\|\sigma_b\|$
1	−43	−164	8·772137	314·03/316·85	−214/125	334·06/317·55
2	0	0	8·789013	322·94/322·56	−49/37	337·33/322·50
3	1648	0	7·252300	705·35/334·85	−326/359	751·41/344·27
4	−43	−15	8·799282	339·18/321·95	−10/11	345·39/321·76
5	0	0	8·800847	333·57/322·56	−11/13	344·40/322·25
6	1648	0	8·796626	320·33/334·85	−22/18	342·12/335·59

Table VI. Western crossing result summary [liquefaction altered seabed profile; $|\sigma_b|$ in (N/mm^2) and H_d in (kN); H_p and H_a same as in Table V; ω in (rad/s)]

	Static analysis			Dynamic analysis		
No.	ΔH_a (kN)	J_s (m)	$\max\|\sigma_b\|/\lim\|\sigma_b\|$	ω_1/ω_3	$\min H_d/\max H_d$	$\max\|\sigma_b\|/\lim\|\sigma_b\|$
1	364	8·809658	205·31/312·92	0·395/1·262	−700/695	283·19/304·06
2	1065	8·898923	260·16/277·88	0·696/2·596	−459/438	302·64/261·09
3	394	7·292996	931·01/351·40	0·575/1·852	−402/432	999·82/359·22
4	3243	9·133696	465·35/185·85	1·435/4·853	−365/352	517·04/196·57
5	3888	9·201648	519·82/159·42	1·371/4·553	−331/336	564·03/163·73
6	2526	9·057136	518·50/321·04	1·413/4·666	−419/514	575·37/335·01

slope was precluded,[6] a gravel surcharge (rip–rap) solution was adopted, which drastically reduced (Figure 7) the peak static bending stresses of concern. Stresses generally remain below the limiting value for the Eastern crossing, whereas for the Western crossing violations of 7 per cent peak magnitude take place in the x-range of 450–480 m, indicating that a probable *in situ* seabed smoothing procedure is in order at these

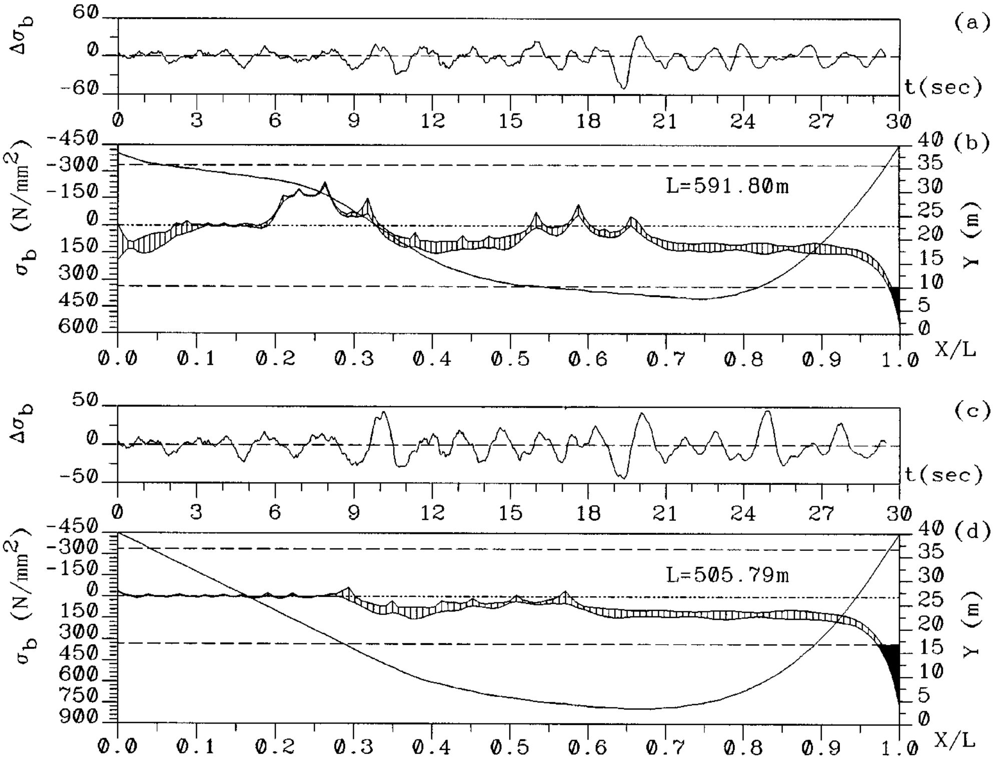

Figure 6. Relative peak dynamic–static bending stress temporal variation and bending stress envelope for Eastern (a), (b) and Western (c), (d) crossing, respectively; no surcharge imposition; pressure test case; natural seabed profile

points. However, the 7 per cent transgression of the stress limits does not cause any undue concern, mainly due to the fact that Det Norske Veritas[16] allows for an 18 per cent increase of the permissible stresses ($1/f_b = 1/0{\cdot}85$).

Loss of surcharge

During earthquake tremors, a loss of surcharge may be experienced at any point along the subsea route of the pipelines. An investigation was therefore carried out, whereby the gravel cover was gradually removed, starting from the critical Revithoussa island boundary, until complete dispersal. A rather susprising numerical result was subsequently obtained (Figure 8), which revealed, firstly that the Eastern crossing was relatively unaffected by the loss of surcharge, and secondly that only the uncovering of the last 100 m of the Western crossing route influenced to any significant extent the peak bending stresses. The main reason for this numerical performance, lies with the increased initial J_s value, obtained after rock dumping, which in turn introduces beneficial compressive forces during surcharge removal.

Seabed soil liquefaction

Extensive *in situ* geotechnical investigations led to the conclusion that the sea floor consisted of a sedimentary layer of variable thickness, being underlain by limestone bedrock. A large proportion of the seabed surfacial layer (Figure 1) was composed of a mixture of silty sand with gravel and clay, which may be classified as loose cohesionless soil being susceptible to possible liquefaction (gradual pore pressure increase leading to shear strength failure) in the event of strong motion earthquakes.

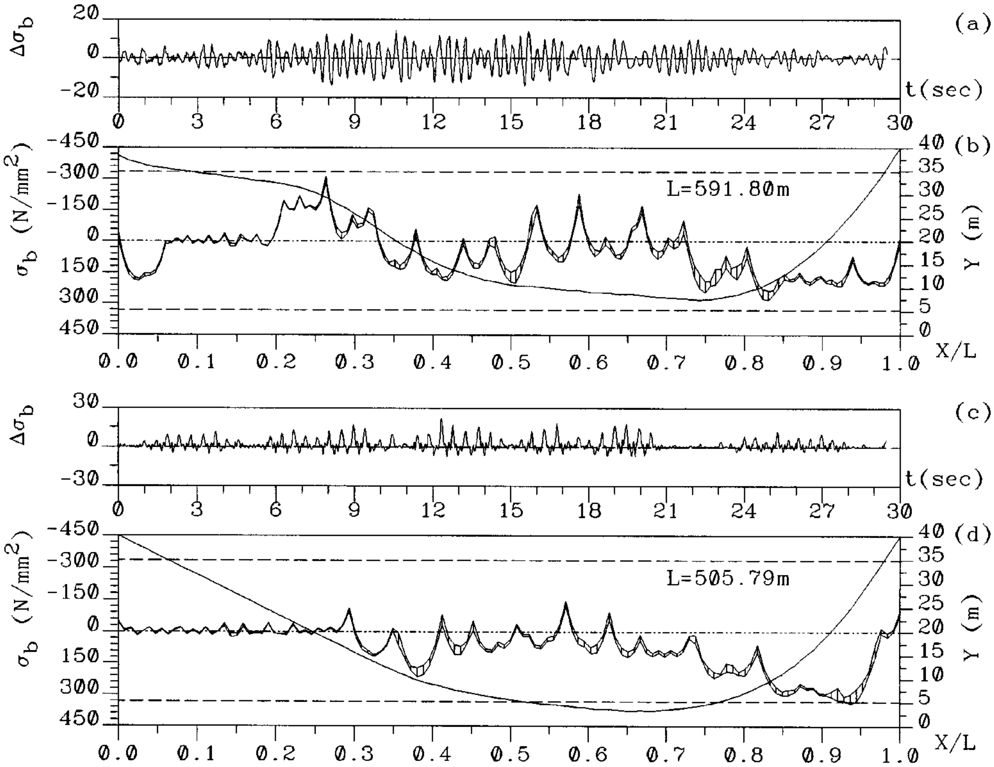

Figure 7. Relative peak dynamic–static bending stress temporal variation and bending stress envelope for Eastern (a), (b) and Western (c), (d) crossing, respectively; gravel surcharge imposition ($S/L = 1{\cdot}0$); pressure test case; natural seabed profile

The modelling of the seabed soil liquefaction phenomenon,[19] beyond the monitoring of horizontal displacements and shear stress values along vertical soil columns, presents a formidable numerical task, since the resulting soil mass flow characteristics are not known beforehand or in general cannot be predicted with any certainty. For argument sake, one could assume instantaneous loss (a severe and unrealistic situation) or, even better, exponential soil dissipation in the surrounding areas by using appropriate parameters, with little to none whatsoever physical significance. The author believes, that such a phenomenon would take place slowly. As a consequence, one is only interested in the stresses induced upon the pipelines by the final non-changeable seabed configuration.

The soil removal, causes the introduction of an additional tensile force ΔH_a due to horizontal motion restraint at the boundary points. These tensions tend to be large in magnitude, therefore leading to low permissible stress limits, particularly when the hoop stresses are either low in absolute value or non-existent (i.e. loading cases 4 and 5). Apart from the empty no surcharge case 1, all other cases indicate severe stress violations, which are more pronounced in the vicinity of rock outcrops. Typical results are given in Tables IV and VI for the Eastern and Western crossing, respectively. For the sake of uniform presentation the pressure test case 6 bending stress results are only illustarted (Figure 9). In this particular test sequence, the waterfilled case 5 proved to be more critical (lack of hoop stresses). The level of peak bending stresses thus determined, indicate that major intervention upon the seabed profile was necessary, in order to avoid the serious economic repercussions that would incur, following pipeline failure due to an earthquake generated seabed profile alteration.

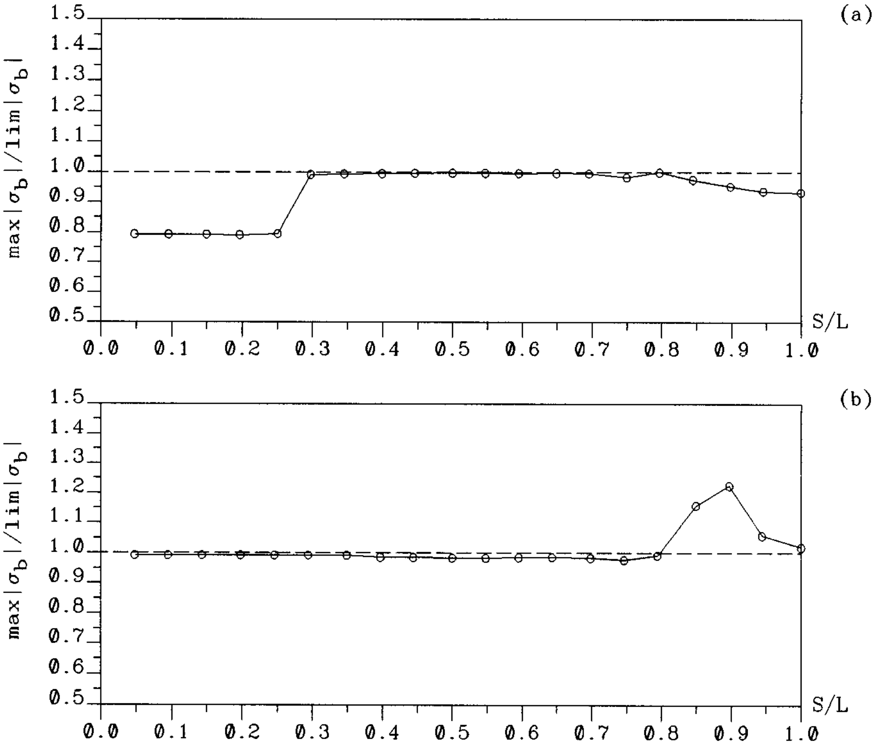

Figure 8. Effect of surcharge loss during an earthquake upon the peak dynamic to allowable bending stress ratio; (a) Eastern, (b) Western crossing; pressure test case; natural seabed profile

CLOSING REMARKS

Point iterative finite element methods enable a rapid and reliable assessment of the dynamic bending stress stability of submarine pipelines in random contact with seabed profiles. Relaxation factors of 1·97 for static and 1·0 for dynamic simulations, yield generally optimal convergence speed. An under-relaxation scheme is necessary, when calculating the axial forces that arise from horizontal motion restrictions. Proper selection of successive iteration force weighting parameters is imperative, if numerical solution divergence is to be avoided. Suggested values range from 0·01 to 0·25, and are strongly influenced by the shape of the seabed profile, the effective pipeline weight, and the length of surcharge cover. Impact–rebound phenomena during pipeline vibrations are efficiently modelled with the aid of an average coefficient of restitution, which represents a mean elastoplastic type of collision. Structural damping may be included in the analysis, if statically determined support points are considered for the calculation of the eigenvalues. For concrete coated submarine steel pipelines a damping ratio of 3 per cent is considered as an appropriate choice. On the whole, the stability of submarine pipelines laid along strait-crossings is assured, if the end points are welded to the mainland sections, following waterfilling and surcharge imposition. In this way the relative distance between the pipe and the sea floor is diminished offering two advantages. First, critical stress points along the irregular subsea route can easily be identified and smoothed out *in situ*, and second, there is greater tolerance against partial loss of protective cover, during seismic excitations. However, measures must always be taken with subsequent major interventions upon the seabed configurations, when the upper sea floor layers within the perspective pipe laying area, are susceptible to mass movements due to large magnitude earthquakes.

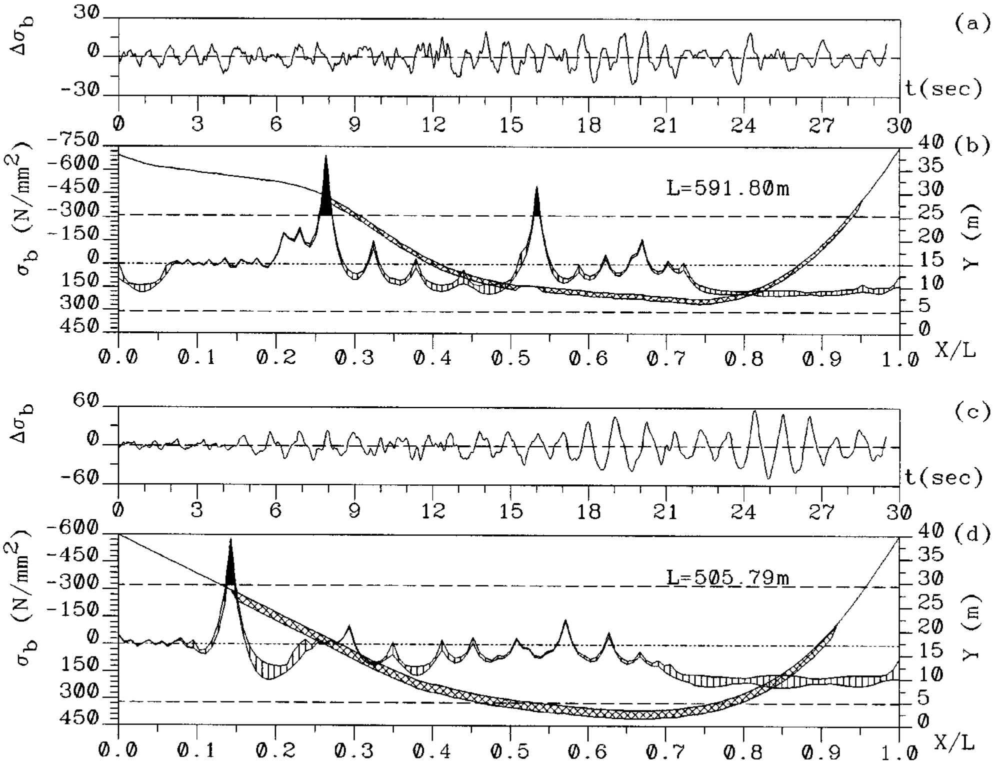

Figure 9. Relative peak dynamic–static bending stress temporal variation and bending stress envelope for Eastern (a), (b) and Western (c), (d) crossing, respectively; gravel surcharge imposition ($S/L = 1{\cdot}0$); pressure test case; altered seabed profile due to soil liquefaction (cross-hatched area)

ACKNOWLEDGEMENTS

The author wishes to acknowledge the valuable comments by the three anonymous reviewers, who indirectly assisted in shaping the manuscript in its present form. In particular, the author acknowledges the first reviewer's exquisite remarks, specifically on the correct form of the restitution equation, the second reviewer's directive for introducing into the analysis an axial force due to horizontal motion restraint and the third reviewer's recommendation towards a more concise exposition of the essential aspects of the theory, including an interesting comment on the contribution of concrete cracking to the damping mechanism. Furthermore, the immediate and decisive intervention by Professor Chopra, in resolving the initial conflicting recommendations, is greatly appreciated by the author.

REFERENCES

1. G. Maier and F. Andreuzzi, 'Elastic and elasto-plastic analysis of submarine pipelines as unilateral contact problems', *Comput. Struct.* **8**, 421–431 (1978).
2. G. E. Stavroulakis, C. C. Baniotopoulos and P. D. Panagiotopoulos, 'Seabed–structure interaction in the presence of frictional effects for submarine pipelines', *Comput. Struct.* **24**(5), 767–775 (1986).
3. P. H. Chuang and D. L. Smith, 'Elastic analysis of submarine pipelines', *J. Struct. Engng. ASCE* **118**(1), 90–107 (1992).
4. S. Bianchi and V. Oliveri, 'Pre-sweeping optimized by mathematical model simulations', *Proc. 7th Int. Conf. on Offshore Mechanics and Arctic Engineering*, Houston, ASME, Vol. 5, 1988, pp. 193–204.
5. C. Kalliontzis, E. Andrianis, K. Spyropoulos and S. Doikas, 'Finite element stress analysis of unilaterally supported submarine pipelines', *Comput. Struct.* **61**(6), 1207–1226 (1996).
6. C. Kalliontzis, E. Andrianis, K. Spyropoulos and S. Doikas, 'Nonlinear static stress analysis of submarine high pressure pipelines', *Comput. Struct.* **63**(3), 397–411 (1997).

7. T. K. Datta and E. A. Mashaly, 'Seismic response of suspended spans of submarine pipeline', *Proc. 7th Int. Conf. on Offshore Mechanics and Arctic Engineering*, Houston, ASME, Vol. 5, 1988, pp. 131–138.
8. R. Romagnoli and R. Varvelli, 'An integrated seismic response analysis of offshore pipeline-sea floor systems', *Proc. 7th Int. Conf. on Offshore Mechanics and Arctic Engineering*, Houston, ASME, Vol. 5, 1988, pp. 139–145.
9. N. G. Figarov and A. M. Kamyshev, 'Seismic stability of offshore pipelines', *Proc. 6th Int. Offshore and Polar Engineering Conf.*, Los Angeles, ISOPE, Vol. 2, 1996, pp. 477–481.
10. A. V. Avdelas, C. C. Baniotopoulos and P. D. Panagiotopoulos, 'Numerical treatment of the sea bed-long underwater cable dynamic interaction problem by an upper bounding algorithm', *Comput. Struct.* **48**(6), 1033–1039 (1993).
11. A. A. Moinfar, A. Naderzadeh, A. Mobinipoor, M. R. Siyah-Kola and M. A. Assar, Accelerograms of the Manjil Iran Earthquake of 20 June 1990, Building and Housing Research Center, Teheran, 1991.
12. A. K. Chopra, *Dynamics of Structures: Theory and Applications to Earthquake Engineering*, Prentice Hall, Englewood Cliffs, NJ, 1995.
13. P. J. M. Lapidaire, 'Statics and dynamics of pipeline spans', *Proc. 4th Int. Conf. on Behaviour of Offshore Structures*, Delft, Elsevier, 1985, pp. 729–738.
14. M. Irvine, *Cable Structures*, Dover, New York, 1992.
15. D. T. Tsahalis and W. T. Jones, 'Scaling of the vortex-induced vibrations of a flexible cylinder near a plane boundary due to steady and wave-induced currents', *Proc. 5th Int. Conf. on Offshore Mechanics and Arctic Engineering*, Tokyo, ASME, Vol. 3, 605–612 (1986).
16. Det Norske Veritas, *Rules for Submarine Pipeline Systems*, Oslo, 1981.
17. M. W. Braestrup and L. W. Andersen, 'Shakedown stress analysis of pressurized pipelines subjected to bending', *Proc. 12th Int. Conf. on Offshore Mechanics and Arctic Engineering*, Glasgow, ASME, Vol. 5, 57–66 (1993).
18. J. N. Reddy, *An Introduction to the Finite Element Method*, McGraw-Hill,New York, 1993.
19. M. S. Rahman, Instability and movement of oceanfloor sediments: a review, *Int. J. Offshore and Polar Engng.* **7**(3), 220–225 (1997).